# Microfluidic elongation of viscous droplets at vanishing interfacial tension

Thomas Cubaud

Phys. Rev. Fluids **8**, 104201 — Published 25 October 2023

DOI: 10.1103/PhysRevFluids.8.104201

# Microfluidic Elongation of Viscous Droplets at Vanishing Interfacial Tension

Thomas Cubaud[1]

*Department of Mechanical Engineering, Stony Brook University, Stony Brook, NY 11794 USA*

**ABSTRACT**

The microflow behavior of liquid-liquid dispersions is experimentally investigated in the presence of miscible fluid additives. Original microfluidic methods are developed to characterize the dynamic response of mobile droplets to a local change of interfacial tension with the external phase using sequential injections and stratified flows. Various oil-alcohol combinations are examined to unravel out-of-equilibrium fluid interactions at short time-scales and clarify the role of flow rates and fluid properties on individual droplet deformations. Functional relationships are developed to characterize the initial droplet strain as well as rates of elongation during immersion and submersion stages in hydrodynamic focusing junctions. It is shown, in particular, that the droplet deformation process is highly non-linear with the initial droplet size and that droplet growth coefficients remain constant for fluid additives having ultra-low interfacial tension. Overall, this study shows the possibility to manipulate the morphology of strongly elongated droplets to enhance oil interfacial area in miscible organic solvents using microchannels.

[1] Author to whom correspondence should be addressed.
Email address: thomas.cubaud@stonybrook.edu

## I. INTRODUCTION

Fluid interfaces are known to behave in varied ways depending on liquid properties and flow conditions [1]. For instance, the spontaneous formation of droplets from a liquid stream results from the competition of surface tension and viscous forces [2-4], and numerous interfacial phenomena of industrial and scientific interests, such as droplet coalescence [5-7] and dynamic wetting [8-10], are commonly observed at the small scale. In general, fine control of droplet dynamics is essential to a range of applications in the field of emulsions [11], and flow-induced deformations of individual droplets have been studied in various configurations [12-17]. In liquid-liquid systems, interfacial tension and solubility largely depend on the polarity of fluid molecules, and a substance affinity toward oil and water is usually characterized using the hydrophilic-lipophilic balance [18]. Alcohol compounds display intriguing interfacial properties as long-chain, fatty alcohols are typically employed as surfactants in water-oil systems and short-chain alcohols find uses such as fuel additives, antiseptics, or solvents for both oil and aqueous phases [19]. As a result, fluid systems made of oils and alcohols display various degrees of solubility and offers opportunities for the elaboration of complex oil mixtures. In general, the development of advanced flow processing techniques of oils and alcohols is important for the industry, such as in the energy and pharmaceutical sectors. In terms of multiphase flows, however, fluid phenomena associated with the introduction of miscible solvents to immiscible liquid-liquid dispersions are poorly understood. In addition, while numerous studies have addressed the thermodynamic stability of ternary mixtures [20-22], including spontaneous emulsification [23-26], at long time-scales, little is known about the behavior of mobile droplets in varying physico-chemical environments at short time-scales.

Here, the dynamic response of viscous droplets to a sudden change of interfacial tension with the external phase is systematically examined in microchannels. Microfluidic platforms enable precise manipulations of droplets [27-30] with fine control over arrangement, size, and velocity [31-34]. The combination of flow rate-controlled droplets and fluid injection scheme provides access to a wide range of flow regimes and hydrodynamic instabilities at various time-scales [35-39]. In this work, fluids are sequentially introduced into a microchannel to examine out-of-equilibrium behavior of ternary systems made of oil and alcohols at short-time scales, *i.e*, at large Péclet number when diffusion phenomena are negligible. The approach consists in generating oil droplets in an immiscible, hydrophilic alcohol phase and combining these streams with a miscible alcohol phase further downstream to form laminar stratifications having vanishing interfacial tension with the droplet. Upon entering stratifications, droplets are rapidly enveloped by the miscible phase and are seen to strongly elongate depending fluid properties and flow conditions. Various aspects of droplet deformation, including immersion and submersion stages, are systematically examined to better characterize the relationship between fluid properties and droplet dynamics at large capillary numbers. It is shown, in particular, that the droplet deformation process is a highly non-linear with the initial

droplet size. Functional relationships based on flow rates and fluid properties, including viscosities and interfacial tensions, are developed to characterize the initial droplet strain as well as rates of elongation at ultra-low interfacial tension. Experiments are conducted for both positive and negative interfacial tension gradients to measure coefficients and factors of elongation for a wide range of fluid properties in the immersion stage. It is also shown that droplets can either elongate or recoil in the submersion stage. Overall, this study shows methods for manipulating the interfacial area of viscous droplets in a variety of organic solvents and clarifies the role of flow rates on droplet deformation at vanishing interfacial tension.

## II. EXPERIMENTAL METHODS

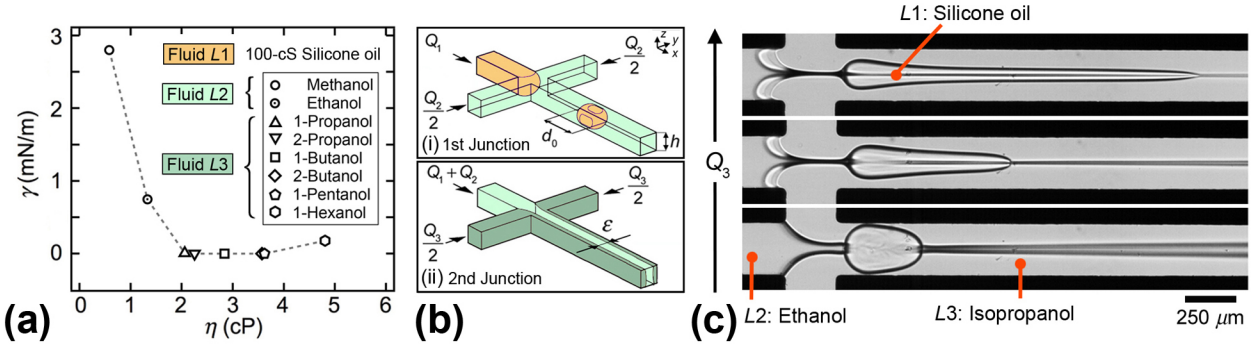


FIG. 1. Fluid properties and experimental apparatus. (a) Interfacial tension $\gamma$ between 100-cS silicone oil and low-molecular weight alcohols as a function of viscosity $\eta$. (b) Schematics of two-step microfluidic injection process with (i) droplet formation of size $d_0$ at the first junction and (ii) alcohol stratifications of width $\varepsilon$ at the second junction. (c) Micrographs of elongated droplets downstream from the second junction for fixed initial droplet size $d_0/h$ = 1.25, fluid pair $E3$-2, flow rates in $\mu$l/min, ($Q_1$, $Q_2$) = (1, 10) and various $Q_3$ = 25, 150, and 200 (from bottom to top).

The dynamic response of a viscous droplet swept away in a miscible environment is examined using a liquid $L1$ for the droplet made of a conventional silicone oil (Gelest) having kinematic viscosity $\eta_1$ = 100 cSt and continuous phases $L2$ and $L3$ made of a variety of low-molecular weight alcohols. Despite their relatively simple molecular structures, alcohols compounds were previously found to be immiscible with $L1$ with small values of $\gamma$ for low carbon numbers $C$ including, methanol, ethanol, and 1-propanol, as well as for large $C$, such as 1-hexanol [40]. By contrast, for moderate $C$, compounds such as 2-propanol, 1- and 2-butanol, as well as 1-pentanol, are miscible with the 100-cSt PDMS oil [41]. Hence, given their small interfacial tension $\gamma$ with the oil, methanol and ethanol are chosen for the initial continuous phase $L2$, and higher molecular weight alcohols are elected for the additive phase $L3$ due to their negligible $\gamma$ with the oil, as can be seen in Fig. 1(a).

Microchannels are made of etched-through silicon wafer of height $h$ = 250 $\mu$m sealed between two borosilicate glass slides using an anodic bonding technique [42]. Such non-deformable microfluidic platforms offer excellent chemical resistance to organic solvents and permit clear optical access for scientific inquiries. Fluids are continuously injected into the device using syringe pumps at flow rates $Q_1$, and $Q_2$, and $Q_3$ for fluids $L1$, $L2$ , and $L3$. All microchannels are square in cross-section of width $h$ and intersect perpendicularly at two junctions. Schematics of the two fluid junctions are shown in Fig. 1(b). The first fluid contactor is used to combine $L1$ and $L2$ and form droplets of $L1$ having size $d_0$ in a continuous phase of $L2$. The flow rate of $L1$ is kept constant at $Q_1$ = 1 $\mu$l/min and $Q_2$ is adjusted in the dilute regime, *i.e.*, $Q_1 \ll Q_2$, to generate small droplets $d_0/h$ approximately ranging between 1 and 2.5. The second hydrodynamic focusing section is employed to symmetrically inject the additive fluid $L3$. Flow rate $Q_3$ is modulated to form stable stratifications of width $\varepsilon_0$ with the initial continuous phase $L2$.

The module is placed on top of an inverted microscope mounted with a high-speed camera and a fiber light is positioned above the chip to provide enough illumination for short-exposure ~ 30 $\mu$s with a fast image acquisition system varying between 250 and 3 000 frames per seconds depending on flow rates. Examples of dynamic droplet deformation in miscible strata are displayed on Fig. 1(c). In this case, droplets have a similar initial size $d_0/h$ = 1.25, which is set by fixing $Q_1$ and $Q_2$, and flow rate $Q_3$ is increased for the fluid pair $L2/L3$ made of ethanol and isopropanol. As can be seen, oil droplets undergo significant morphological changes depending on ternary alcohol flow rate $Q_3$. In the following, fluid pairs are labelled according to the scheme $M$ or $E$ for methanol or ethanol as fluid $L2$ and the carbon number and isomers of alcohol compound as $L3$. For instance, the ethanol-isopropanol fluid pair is coded as $E3$-2 and the methanol-hexanol fluid pair as $M6$-1. While this study primarily focuses on the situation where $L3$ is miscible with the oil, systematic investigations are also conducted for cases where $L3$ is immiscible with the oil, for instance with fluid pairs such as methanol-ethanol ($M2$) and ethanol-methanol ($E1$). This method allows to examine flow transition at relatively large initial capillary numbers Ca = $\eta_1 V/\gamma$ and investigate the role of the interfacial tension gradient $\nabla\gamma = (\gamma_{13} - \gamma_{12})/h$, which could be either positive, negative, or null.

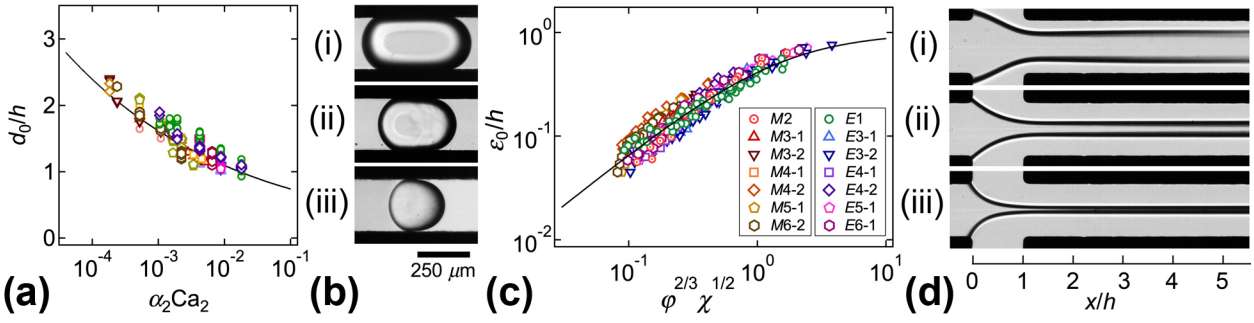


FIG. 2. Initial conditions. (a) Droplet size $d_0/h$ as a function of $\alpha_2 Ca_2$ for all fluid pairs, solid line: $d_0/h = 0.5(\alpha_2 Ca_2)^{-0.17}$(b) Micrographs of droplets in the inlet channel, flow rates ($Q_1$, $Q_2$, $Q_3$) in $\mu$l/min, (i) Fluid pair

*M*4-1 (1, 4, 15), (ii) Fluid pair *E*3-2 (1, 4, 1), and (iii) fluid pair *E*6-1 (1, 20, 20). (c) Width of stable stratifications $\varepsilon_0/h$ as a function of $\varphi^{2/3}\chi^{1/2}$, solid line: $\varepsilon_0/h = 1/[1+(0.7\ \varphi^{2/3}\chi^{1/2})^{-1}]$. (d) Micrographs of stable stratification for fluid pair *E*3-2, (i) (1, 20, 10), (ii) (1, 20, 50), and (iii) (1, 20, 200).

The deformation of droplets in cross-flows is particularly sensitive to injection flow rates, $Q_1$, $Q_2$, and $Q_3$, which set initial conditions – or premises of the experiment – with parameters such as the initial droplet size $d_0$ and the stable stratification width $\varepsilon_0$. In the first junction, monodispersed droplets of size $d_0 \sim h$ are emitted one-by-one and separated by a large spacing $L \gg d_0$ in the dilute regime, *i.e.*, for large *L*2 liquid fraction $\alpha_2 = Q_2/(Q_1 + Q_2)$. The relatively low droplet emission frequency in this case enables the 'healing' of stratifications after the passage of each droplet. As the experimental field of view captures both upstream and downstream from the second junction, $d_0$ and $\varepsilon_0$ are systematically recorded before each droplet immersion in interfacial tension stratifications. Previous work on viscous droplet formation in square microchannels [31] has shown that $d_0/h = 0.5(\alpha_2 \mathrm{Ca}_2)^{-0.17}$, where $\mathrm{Ca}_2 = \eta_2 Q_2/(\gamma_{12}h^2)$ is the capillary number based on *L*2 superficial velocity and viscosity. Current data are compared to this previous scaling and very good agreement is found independently of $Q_3$ [Fig. 2(a)]. Therefore, the size of oil droplets $d_0/h$ produced in either ethanol or methanol can be finely manipulated with $Q_1$ and $Q_2$ and mainly ranges between 1 and 2.5 in this series of experiment [Fig. 2(b)]. Due to the role of the capillary number during droplet formation, large droplets with hemispherical caps are typically produced at low flow rates [Figs. 2(b)(i) and 2(b)(ii)], while small droplets having bullet shapes are generated at larger flow rates [Figs. 2(b)(iii)]. Using a similar approach, the stable strata width $\varepsilon_0$ is compared with preceding work on the stability of miscible stratifications in square channels [43], which showed the importance of the parameter $\varphi^{2/3}\chi^{1/2}$, which here can be written as $\varphi = (Q_1 + Q_2)/Q_3$ for the flow rate ratio and $\chi = \eta_2/\eta_3$ for the viscosity contrast. As can be seen on Fig. 2(c), data collapse onto a master curve delineated by the bounded function $\varepsilon_0/h = 1/[1 + (0.7\ \varphi^{2/3}\chi^{1/2})^{-1}]$ in agreement with previous work. Micrographs of alcohol stratifications *L*2/*L*3 prior to droplet passage are displayed on Fig .2(d) and straight stratifications with negligible diffusive spread are observed over the range of flow rates investigated. In conclusion, initial droplet sizes and strata widths can be finely adjusted with flow rates to systematically examine their role on droplet deformation and particularly for the case of a vanishing interfacial tension between oil and various alcohol compounds.

## III. PHENOMENOLOGY

Droplets entering strongly stratified flows having negligible interfacial tension $\gamma_{13}$ are rapidly engulfed in the solvent *L*3 and undergo complex morphological transitions as they traverse the contactor region and the outlet channel [Fig. 3(a)]. Droplet motion is composed of three stages, including a phase of approach where droplets of size $d_0$ flow toward the second junction at velocity $V_0 \sim (Q_1 + Q_2)/h^2$. The immersion

phase begins when the droplet front reaches the junction edge at $x/h = 0$ and makes first contact with the flow of solvent $L3$ symmetrically injected at $Q_3$. At this stage, the droplet nose elongates in the form of a cusp due to the local hydrodynamic focusing and droplets experience an overall rapid elongation as they further enter the junction. Finally, the submersion phase is attained when the droplet rear moves past $x/h = 0$. At this point, a significant portion of each droplet is coated with fluid $L3$ and droplets continue to slowly deform as they are convected in the outlet microchannel.

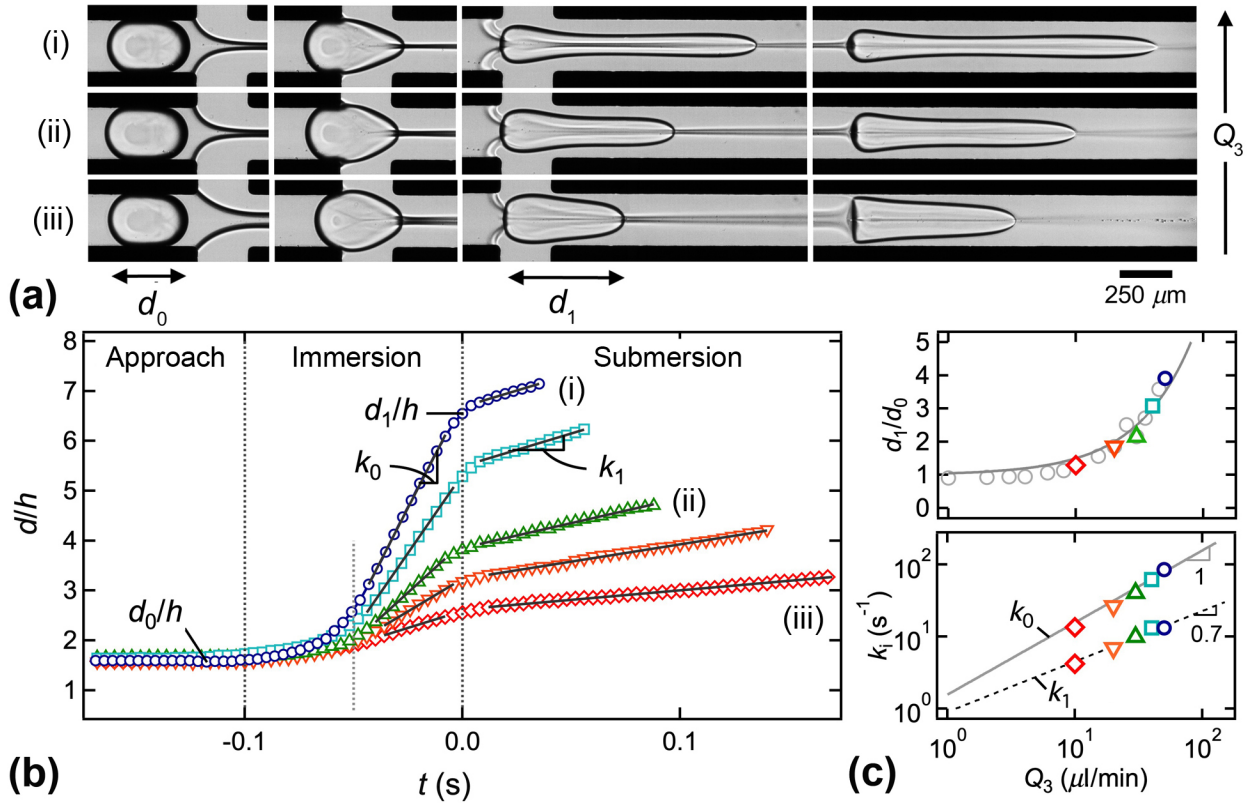


FIG 3. Evolution of droplet deformation in interfacial tension strata, fluid pair $E3$-2, flow rates in $\mu$l/min, $Q_1$ =1 and $Q_2 = 4$, (a) Time-series of various deformation stages for fixed droplet size $d_0/h = 1.64$ and various $Q_3$ = (i) 50, (ii) 30, and (iii) 10. (b) Droplet length $d/h$ as a function of time $t$ for $Q_3 = 10$ (◇), 20 (▽), 30 (△), 40 (□), and 50 (○). (c) Top: Evolution of relative deformation $d_1/d_0$ vs. $Q_3$, solid line: $d_1/d_0 = 1 + 0.05Q_3$. Bottom: Measurement of rates of elongation $k_0$ and $k_1$ vs. $Q_3$, solid lines: $k_0 = 1.56Q_3$, $k_1 = 0.90Q_3^{0.7}$.

To better understand this process for a given fluid pair, we first focus the role of flow rate $Q_3$ and examine the evolution of the droplet width $d$ for similar initial droplet sizes $d_0$, *i.e.,* for fixed values of $Q_1$ and $Q_2$. The instantaneous width $d$ is extracted from spatiotemporal diagrams of high-speed movies and shown as a function of time $t$ in Fig. 3(b) for fluid pair $E3$-2. To compare droplet elongation data, the clock is set at $t = 0$ when the droplet fully enters the junction at $x/h = 0$, *i.e.*, at the beginning of the submersion stage. The temporal evolution of $d/h$ at the beginning of the immersion stage reveals that a droplet first

slowly extends until its front cap reaches the outlet channel at $x/h = 1$, after which a linear increase of $d/h$ with time is observed at rate $k_0$. In the following, we refer to $k_0$ as the immersion rate [Fig. 3(b)]. Subsequentially, when the droplet has fully entered the junction, *i.e.*, at the transition between the immersion and the submersion stages, the droplet width $d$ has grown from $d_0$ to $d_1$ before slowly extending at submersion rate $k_1$ in the outlet channel.

Overall, fixing the initial droplet size $d_0$ and varying $Q_3$ for a given fluid pair shows a smooth evolution of our three quantities of interest, including elongation rates $k_0$ and $k_1$ as well as elongation width $d_1$ [Fig. 3(c)]. In particular, the droplet relative elongation $d_1/d_0$ is reasonably well fitted with a function of the form $1 + a_0 Q_3$, where $a_0$ is a constant. For very low $Q_3$, droplets slightly grow laterally due to the presence of side openings channels and 'weak' hydrodynamic focusing at the junction, which leads to $d_1$ being less than $d_0$ [Fig. 3(c) - top] Such behavior corresponds to the lower limit of proposed modelling and is neglected in the following. Finally, for this specific set of flow rates, the experimentally measured rate of elongation $k_0$ appears linear with $Q_3$ while $k_1$ scales with $Q_3^{0.7}$.[Fig. 3(c) - bottom]. In general, the relatively simple dependencies of droplet deformation parameters, $d_1$, $k_0$, and $k_1$, with $Q_3$ when all other parameters are fixed provide a basis for comparing the roles of the initial droplet size $d_0$ and interfacial fluid properties.

## IV. INITIAL ELONGATION

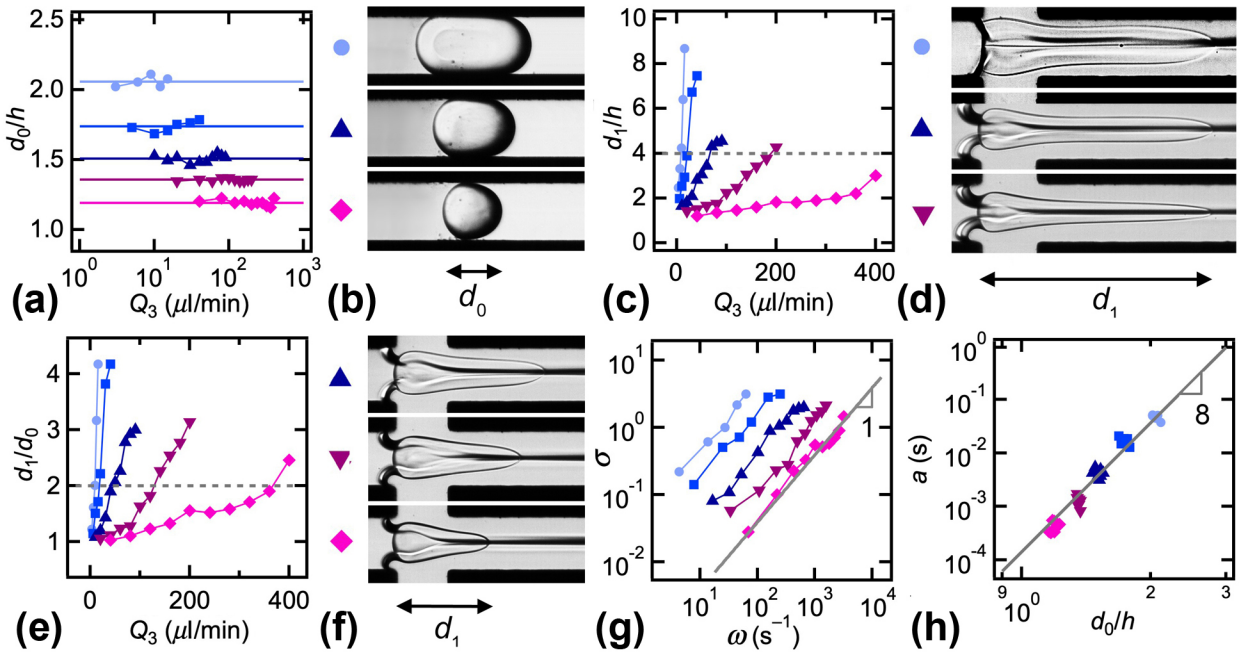


FIG 4. Role of initial size $d_0$ on droplet deformation $d_1$, fluid pair *E*4-2, flow rates in μl/min. (a) Initial size $d_0/h$ versus $Q_3$ for various ($Q_1$, $Q_2$): (1, 3) (●), (1, 5) (■), (1, 10) (▲), (1, 20) (▼), (1.40) (◆). (b) Micrographs of initial droplets for $d_0/h = 2.06$ (●), 1.51 (▲), 1,19 (◆). (c) Elongation $d_1/h$ as a function of $Q_3$. (d) Micrographs of elongated droplets for $d_1/h \sim 4$, ($Q_1$, $Q_2$, $Q_3$) = (1, 3, 9) (●), (1, 10, 80) (▲), and (1, 20, 200) (▼). (e) Relative

deformation $d_1/d_0$ vs. $Q_3$. (f) Micrographs of elongated droplets for $d_1/d_0 \sim 2$, from top to bottom ($Q_1$, $Q_2$, $Q_3$) = (1, 10, 50) (▲), (1, 20, 120) (▼) , and (1, 40, 360) (◆). (g) Strain $\sigma$ as a function of effective shear rate $\omega$, solid line: $\sigma = a\omega$, where $a = 3.9\times10^{-4}$ s. (h) Coefficient of elongation $a$ vs. initial size $d_0/h$, solid line: $a = \xi (d_0/h)^8$, where $\xi = 1.4\times10^{-4}$ s.

The microfluidic deformation of droplets is a highly non-linear process with respect to the initial droplet size $d_0$. To further quantify the influence of $d_0$ on elongation $d_1$, we focus on the data set associated with fluid pair *E*4-2, where five different $d_0$ are produced for fixed values of $Q_1$ and $Q_2$ while $Q_3$ is varied [Fig. 4(a)]. It is shown in particular that since flow rates are separately imposed with syringe pumps using incompressible fluids, the initial droplet size $d_0$ remains independent of downstream injection flow rate $Q_3$. As the typical field of view includes the outlet channel length of about $10h$ and droplets strongly elongate, we examine a rather narrow range of $d_0/h$ between 1 and 2 [Fig. 4(b)]. The corresponding absolute deformations $d_1/h$ are measured as a function of $Q_3$ and shown in Fig. 4(c). It is evident from this graph that droplets with large $d_0$ are strongly deformed at low $Q_3$ and droplets with small $d_0$ are weakly deformed at large $Q_3$. Micrographs of elongated droplets for fixed $d_1 \sim 4h$ and various $d_0$ are displayed in Fig. 4(d) and show significant variations in droplet morphologies, with nearly constant lateral width for large $d_0$ and droplets with rounded back and pointed front for small $d_0$. It is found, however, that for fixed relative deformation $d_1/d_0 \sim 2$, droplets of different initial sizes display similar shapes, which roughly differs by a size factor [Figs. 4(e) and 4(f)]. Hence, since data show that $d_1/d_0 \sim 1$ for $Q_3 \sim 0$, the droplet elongation parameter $\sigma = d_1/d_0 - 1$, *i.e.*, the droplet strain, is expected to scale linearly with $\sigma \sim Q_3$. In addition, as droplet are confined in a central steam of width $\varepsilon$, simple mass conservation in the presence of stratifications indicates that $d_0h^2 = d_1h\varepsilon$, which yields $\sigma \sim h/\varepsilon - 1 \sim \varphi^{-2/3}\chi^{-1/2}$. Combining arguments leads to the formulation of the effective shear rate $\omega = \varphi^{-2/3}\chi^{-1/2}Q_3/h^3$, which enables quantification of droplet strains according to $\sigma = a\omega$, where the coefficient of elongation $a$ depends on initial droplet size $d_0/h$. [Fig. 4(g)]. To probe the relationship between strain and initial droplet size, the coefficient $a = \sigma/\omega$ is calculated for each droplet and plotted as a function of $d_0/h$ in Fig. 4(h). Results show a very strong influence of initial size on elongation according to $a \sim \xi(d_0/h)^8$, where the factor of elongation $\xi$ is characteristic to each fluid pair and depends on fluid properties. Previous work on microfluidic droplet elongation in two-fluid systems also show significant non-linearities with $d_0/h$ [16].

Deformed droplets adopt a range of complex shapes that are difficult to predict based on interfacial tensions $\gamma_{12}$ and $\gamma_{13}$. Therefore, the method of determining the elongation factor $\xi$ for each fluid pair provides a basis to quantify the role of interfacial properties on droplet strains. Hence, we generalize the technique

of plotting coefficients $a$ versus $d_0/h$ to all experiments and calculate the specific elongation factor $\xi$ associated with each fluid pair (Fig. 5). It is found, in particular, that for a given initial phase $L2$, *i.e.*, ethanol or methanol, the measured factors $\xi$ remain similar when $\gamma_{12} \gg \gamma_{13}$, with an average value of $\xi_E \sim 1.78\times10^{-4}$ s for ethanol [Fig. 5(a)] and $\xi_M \sim 3.57\times10^{-5}$ s for methanol [Fig. 5(b)]. For comparison, elongation factors are plotted as a function of the viscosity of the solvent $L3$ for all fluid pairs in Fig. 5(c). For the cases of vanishing interfacial tension $\gamma_{13} \sim 0$, micrographs of elongated droplets for similar initial droplet sizes $d_0/h$ at various $Q_3$ are shown on Figs 5(d) and 5(e). Droplet morphologies with similar $d_1/h$ are obtained when $L2$ is ethanol or methanol, however, with significant differences in flow rates. For instance, a much larger $Q_3$ is needed when $L2$ is methanol to match droplet morphologies found when $L2$ is ethanol. It is also instructive to examine cases with non-negligible $\gamma_{13}$, where elongation factor $\xi$ are found at lower values for cases $E1$ ($\gamma_{12} < \gamma_{13}$) , $E2$ ($\gamma_{12} = \gamma_{13}$), and $M2$ ($\gamma_{12} > \gamma_{13}$) [Fig. 5(c)]. Typical deformed droplet morphologies are displayed on Fig. 5(f) when droplets are exposed to a positive interfacial tension gradient $\nabla\gamma > 0$ and form curved front caps. Incidentally, the fact that positive strains are found in this situation exemplifies the interplay between bulk viscous forces and interfacial capillary forces at hydrodynamic focusing sections.

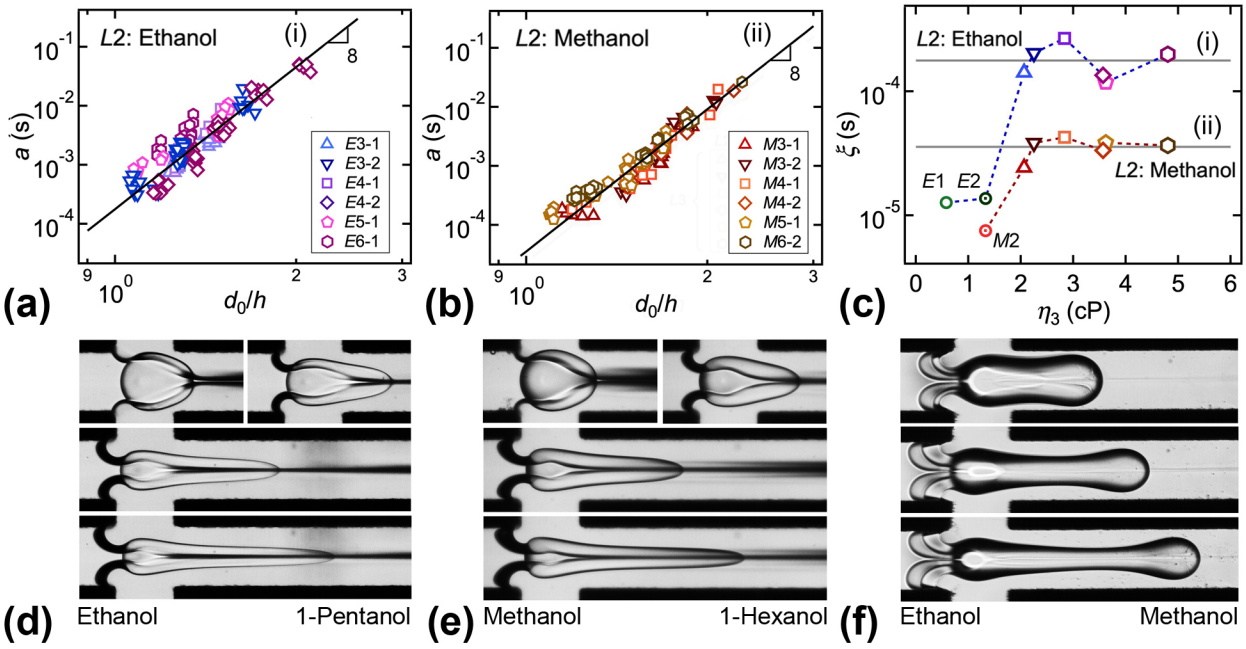


Fig. 5. (a) Coefficient of elongation $a$ as a function of $d_0/h$ when $L2$ is made of ethanol. Solid line: $a = \xi_E d_0/h$, where $\xi_E = 1.78\times10^{-4}$ s. (b) Coefficient $a$ vs. $d_0/h$ when $L2$ is methanol. Solid line: $a = \xi_M d_0/h$, where $\xi_M = 3.57\times10^{-5}$ s. (c) Factor of elongation $\xi$ vs. viscosity $\eta_3$ for all fluid pairs. Solid lines: $\xi =$ (i) $\xi_E$ and (ii) $\xi_M$ (d) Micrographs of elongated droplets for fluid pair $E5$-1, flow rates in $\mu$l/min, $(Q_1, Q_2) = (1, 15)$, $Q_3 = 30, 70, 120, 180$ (from top to bottom). (e) Micrographs for fluid pair $M6$-1, $(Q_1, Q_2) = (1, 40)$, $Q_3 = 80, 180, 260, 340$ (from top to bottom). (f) Micrographs for fluid pair $E1$, $(Q_1, Q_2) = (1, 5)$, $Q_3 = 100, 300, 400$ (from top to bottom).

The elongation factor provides a means to characterize droplet morphologies and corresponds to the droplet strain $\sigma$ per unit shear rate $\omega$ for a given initial droplet size $d_0$, $\xi \sim \sigma\omega^{-1}(d_0/h)^{-8}$. This quantity remains relatively constant for a given fluid pair suggesting a function $f$ such as $\xi = f(\gamma_{12}, \gamma_{13})$. It is found experimentally that such function $f$, however, does not appear to scale with the interfacial tension gradient $\nabla\gamma = (\gamma_{13} - \gamma_{12})/h$ or ratio $\gamma_{13}/\gamma_{12}$ but rather depends on an inverse product of $\gamma_{12}$ and $\gamma_{13}$ as $\xi$ is the largest when both interfacial tension are small, as shown in Fig. 6. Indeed, in the cases of favorable interfacial tension gradient $\nabla\gamma < 0$, modest deformations are expected when (a) $\gamma_{12}$ is relatively large and associated with small initial capillary numbers $\mathrm{Ca}_0 = \eta_2 V_0/\gamma_{12}$ [Fig. 6(a)]. In case (b), stratifications having much smaller $\gamma_{13}$ yield larger deformations due to a significant increase of capillary number at the fluid contactor [Fig. 6(b)]. Finally, when $\gamma_{12}$ is relatively small and associated with large initial capillary number $\mathrm{Ca}_0$, very strong deformations are expected in case (c) when droplet enter stratifications having ultra-low interfacial tension $\gamma_{13} \sim 0$ [Fig. 6(c)]. Incidentally, in this example, the interfacial tension gradient is larger in case (b) for fluid pair *M*6-1 compared to case (c) with fluid pair *E*3-2, thereby illustrating the complexity of empirically defining the function $f$. One notes that the ratio of elongation factors between ethanol and methanol for miscible stratifications $\xi_E/\xi_M \sim 5$ is commensurable with the ratio of initial interfacial tension between methanol and ethanol $\gamma_{12M}/\gamma_{12E} \sim 3.7$ highlighting the influence of the initial capillary number on droplet deformation processes in miscible stratifications.

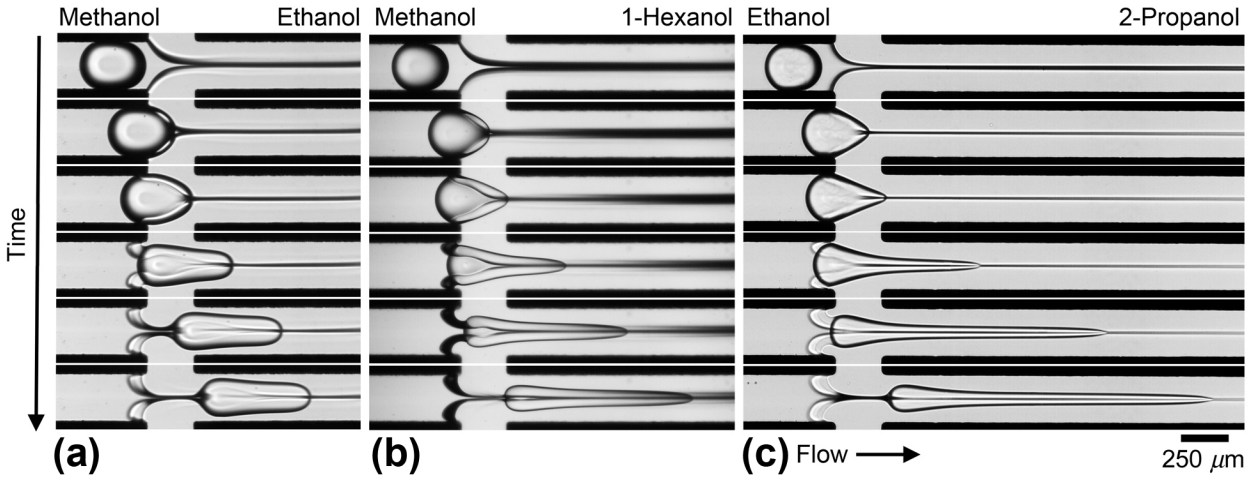


FIG. 6 Influence of elongation factor $\xi$ on droplet morphologies and dynamics, from rounded droplets (low $\xi$) to pointy droplets (large $\xi$). Flow rates in $\mu$l/min. (a) Time-series with fluid pair *M*2, where $\xi \approx 7.5\times10^{-6}$ s, and $(Q_1, Q_2, Q_3) = (1, 40, 400)$. (b) Fluid pair *M*6-1 where $\xi \approx 3.7\times10^{-5}$ s, and $(Q_1, Q_2, Q_3) = (1, 40, 360)$. (b) Fluid pair *E*3-2, where $\xi \approx 2.0\times10^{-4}$ s, and $(Q_1, Q_2, Q_3) = (1, 10, 200)$.

Overall, complexity in defining time-dependent droplet morphologies is also evident through detailed observation of time-series of droplets during the immersion stage. In particular, the development of a lubrication layer of fluid $L3$ progressively enveloping droplets at the junction and resembling 'eyelids' closing on droplets is apparent in Fig. 6. At the beginning of the submersion stage, however, droplets are mostly encapsulated by $L3$ and can experience either a positive or negative elongation rate $k_1$ depending on the sign of the interfacial tension gradient $\nabla\gamma$ as discussed in the next section.

## V. SUBMERGED DROPLETS

The interplay between droplets and stratifications in microchannels can lead to elaborate interfacial flow rearrangements due to significant velocity differences between separated and dispersed flows. Such interaction between droplet shape and structure of separated flows is particularly pronounced for viscous stratifications, such as in the case of high-viscosity layered-flows [44] as well as viscous thread flows [45]. In the present situation where droplets are primarily swept away into interfacial tension stratifications, the central stream made of the initial continuous phase $L2$ typically flows faster than droplets $L1$ and tends to accumulate at the droplet rear, which locally increases $\varepsilon$ in this region. By contrast, in the frontal region, as the droplet velocity is larger than that of the side streams of $L3$, the velocity differential leads to the relative displacement of $L3$ toward the central stream to conserve mass, which closes stratification downstream and locally reduces $\varepsilon$. As a result, in the case of $\nabla\gamma < 0$, submerged droplet adopt the shape of cones with small back curvatures, *i.e.*, flat backs, and large front curvatures with pointy noses [Fig. 7(a)].

To develop deeper insights into the role of interfacial tension on submerged droplets, a systematic analysis of the temporal evolution of the droplet length $d(t)$ is conducted in the outlet channel to calculate the rate of elongation $k_1 = d(d/h)/dt$. For the model fluid pair $E4$-2, it is found that, independently of the initial droplet size $d_0/h$, the rate of elongation scales with the effective shear rate as $k_1 = b\omega^{0.7}$, where the constant $b$ is a characteristic of each fluid pair Fig. 7(b). This scaling approach is generalized to fluid pairs made of ethanol [Fig. 7(c)] and methanol [Fig. 7(d)] as $L2$ to extract the constant $b$ for the case of decreasing interfacial tension, *i.e.,* $\nabla\gamma < 0$. While droplets injected in a lower interfacial tension phase continue to elongate, by contrast, when the fluid $L3$ has a similar or higher $\gamma_{13}$ compared to $\gamma_{12}$, droplets are seen to progressively coil back further downstream. Hence, in the case when $\nabla\gamma \geq 0$, the rate of elongation $k_1$ is negative. Therefore to find the scaling dependency with $\omega$, the coefficient $-k_1$ is fitted with a function $-b\omega^{0.7}$ and negative growth coefficient $b$ are measured for fluid pairs $E1$ and $E2$ [Fig. 7(e)]. Data for fluid pairs with vanishing interfacial tension $\gamma_{13} \sim 0$ show a similar value of $b \sim 0.4$ $s^{-0.3}$ regardless of $L2$ made of ethanol of methanol. This behavior for $k_1$ is in contrast with that of immersed droplets, where the factor of elongation $\xi$ strongly depends on $L2$ [Fig. 5(c)]. This result suggests that most of the droplet initial surrounding phase $L2$ has

been replaced by $L3$ in the submerged stage and that mobilized droplets elongate when abruptly exposed to a miscible phase. More work is required to quantify the role of the droplet viscosity $\eta_1$ on the rates of elongation in the immersed and submerged stages.

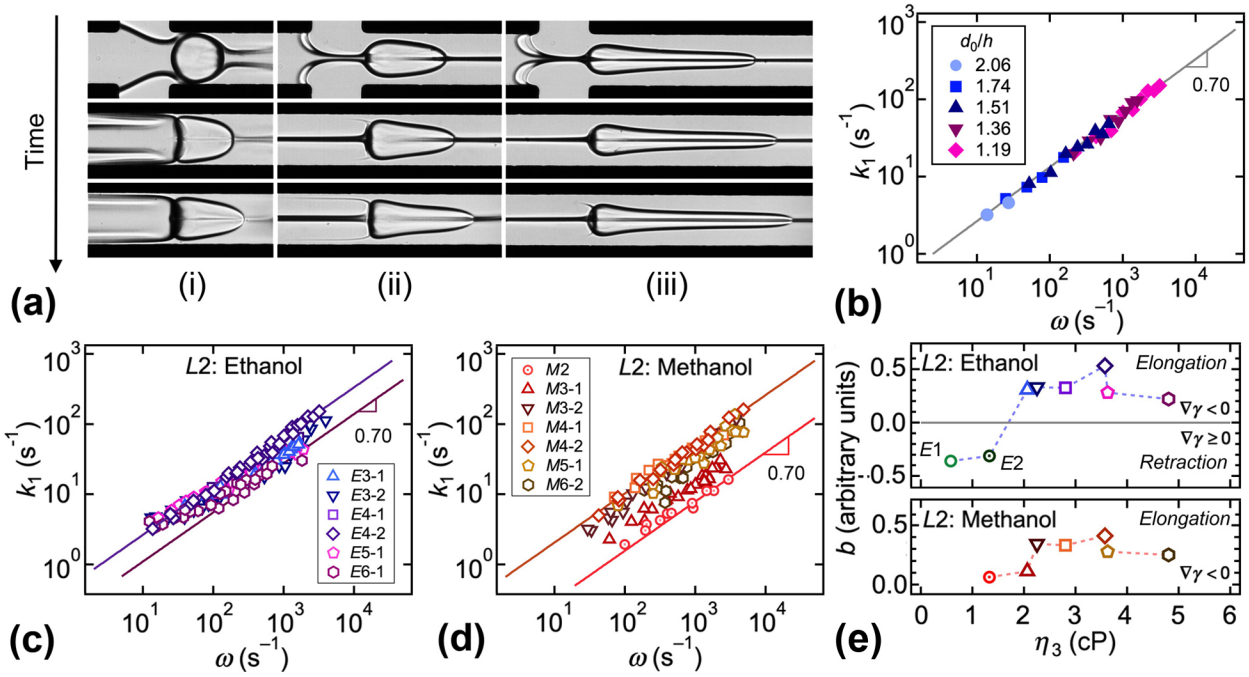


FIG. 7. Submerged droplet evolution in interfacial tension stratifications. (a) Time-series of droplets elongating in the outlet channel for small $d_0/h = 1.10$, fluid pair $E3$-2, flow rates in $\mu$l/min, $(Q_1, Q_2) = (1, 20)$, (i) $Q_3 = 10$ and $\Delta t = 76$ ms, (ii) $Q_3 = 200$ and $\Delta t = 10$ ms, and (iii) $Q_3 = 400$ and $\Delta t = 3.7$ ms. (b) Evolution of elongation coefficient $k_1$ as a function of $\omega$ for fluid pair $E4$-2, solid line: $k_1 = b\omega^{0.70}$ (c) Growth of $k_1$ vs. $\omega$ for fluid pairs where $L2$ is ethanol at vanishing $\gamma_{13}$. (d) Growth of $k_1$ as a function of $\omega$ for fluid pairs where $L2$ is methanol at low $\gamma_{13}$. (e) Growth coefficient $b$ as a function of $\eta_3$ for all fluid combinations.

## VI. CONCLUSIONS

This work examines the evolution of viscous droplets injected into microfluidic stratifications having various interfacial tensions. A two-step hydrodynamic focusing section is employed to continuously generate high-viscosity oil droplets in immiscible alcohols at the first junction and inject droplets into miscible alcohol phases at the second junction. The sudden change in interfacial tension at the solvent contactor induces a range of complex interfacial phenomena causing drops to significantly elongate during the various stages of immersion and submersion into organic solvents. Methods based on scaling relationships are developed to predict and manipulate dynamic droplet elongations for the case of stratifications having ultra-low, *i.e.*, vanishing, interfacial tension with droplets. In particular, the roles of flow rates, initial droplet

sizes, and fluid properties are systematically investigated to probe droplet governing parameters during different periods of continuous phase substitution. It is shown in particular, that the while the droplet strain $\sigma$ strongly depends on the initial interfacial tension $\gamma_{12}$ and initial droplet size $d_0$ during the immersion stage, the rate of elongation in the submersion stage essentially depends on added solvent properties and remains largely independent of segmented flows initial conditions. Future work could consider the role of droplet viscosity $\eta_1$ on microfluidic elongation rates for improving modeling of mobile droplet deformation based on fluid properties. More work is also needed to better characterize wetting and lubricating properties of ternary fluid systems made of oil and alcohols. Numerical inquiries would provide further insights concerning the role of the initial interfacial tension on elongation factors in miscible stratifications. Finally, refinements are needed in the prediction of the transition between droplet elongation and retraction in the submerged stage. Overall, this study shows the possibility to manipulate the morphology of strongly elongated droplets to enhance oil interfacial area in miscible solvents using microchannels.

## ACKNOWLEDGEMENTS

This material is based upon work supported by the National Science Foundation under Grand No. CBET-2223988

## REFERENCES

[1] P. G. de Gennes, F. Brochard-Wyart, and D. Quéré, Capillarity and Wetting Phenomena: Drops, Bubbles, Pearls, Waves (Springer Sciene+Business Media LLC, New York, 2004).

[2] J. Eggers and E. Villermaux, Physics of liquid jets, Rep. Prog. Phys. **71**, 036601 (2008).

[3] J. M. Montanero and A. M. Gañán-Calvo, Dripping, jetting and tip streaming, Rep. Prog. Phys. **83**, 097001 (2020).

[4] B. Ambravaneswaran, H. J. Subramani, S. D. Phillips, and O. A. Basaran, Dripping-jetting transition in a dripping faucet, Phys. Rev. Lett. **93**, 034501 (2004).

[5] J. Eggers, J. R. Lister, and H. A. Stone, Coalescence of liquid drops, J. Fluid Mech. **401**, 293 (1999).

[6] L. G. Leal, Flow induced coalescence of drops in a viscous fluid, Phys. Fluids **16**, 1833 (2004).

[7] J. D. Paulsen, R. Carmigniani, K. A., J. C. Burton, and S. R. Nagel, Coalescence of bubbles and drops in an outer fluid, Nature **5**, 3182 (2014).

[8] C. Duez, C. Ybert, C. Clanet, and L. Bocquet, Making a splash with water repellency, Nature Physics **3**, 180 (2007).

[9] D. Quéré, Wetting and roughness, Ann. Rev. Mater Res. **38**, 71 (2008).

[10] J. H. Snoeijer and B. Andreotti, Moving contact lines: scales, regimes, and dynamical transitions, Annu. Rev. Fluid Mech. **45**, 269 (2013).

[11] F. Leal-Calderon, V. Schmitt, and J. Bibette, Emulsion Science: Basic Principles (Springer, New York, 2007).

[12] B. J. Bentley and L. G. Leal, An experimental investigation of drop deformation and breakup in steady two-dimensional flows, J. Fluid Mech. **167**, 241 (1986).

[13] J.-W. Ha and L. G. Leal, An experimental study of drop deformation and breakup in extensional flow at high capillary number, Phys. Fluids **13**, 1568 (2001).

[14] J. T. Cabral and S. D. Hudson, Microfluidic approach for rapid multicomponent interfacial tensiometry, Lab on a Chip **6**, 427 (2006).

[15] A. Vananroye, P. J. A. Janssen, P. D. Anderson, P. Van Puyvelde, and P. Moldenaers, Microconfined equiviscous droplet deformation: Comparison of experimental and numerical results, Phys. Fluids **20**, 013101 (2008).

[16] T. Cubaud, Deformation and breakup of high-viscosity droplets with symmetric microfluidic cross flows, Phys. Rev. E **80**, 026307 (2009).

[17] A. Z. Zinchenko and R. H. Davis, Motion of deformable drops through porous media, Annu. Rev. Fluid Mech. **49**, 71 (2017).

[18] A. W. Adamson and A. P. Gast, Physical Chemistry of Surfaces (John Wiley & Sons, Inc., New York, 1991).

[19] D. Klein, Organic Chemistry (John Wiley & Sons, Inc., Danvers, 2012).

[20] G. W. Castellan, Physical Chemistry (Addison-Wesley Publishing Company, Reading, Massachusetts, 1983).

[21] R. G. Larson, The Structure and Rheology of Complex Flluids (Oxford University Press, Inc., New York, 1999).

[22] H.-J. Butt, K. Graf, and M. Kappl, Physics and Chemistry of Interfaces (Wiley-VCH, Weinheim, 2006).

[23] N. Shahidzadeh, D. Bonn, J. Meunier, M. Nabavi, M. Airiau, and M. Morvan, Dynamics of spontaneous emulsification for fabrication of oil in water emulsions, Langmuir **16**, 9703 (2000).

[24] S. A. Vitale and J. L. Katz, Liquid droplet dispersions formed by homogeneous liquid-liquid nucleation: "The ouzo effect", Langmuir **19**, 4105 (2003).

[25] C. Solans, D. Morales, and M. Homs, Spontaneous emulsification, Current Opinion in Colloids & Int. Sci. **22**, 88 (2016).

[26] H. Tan, C. Diddens, A. Mohammed, J. Li, M. Versluis, X. Zhang, and D. Lohse, Microdroplet nucleation by dissolution of a multicomponent drop in a host liquid, J. Fluid Mech. **870**, 217 (2019).

[27] R. Seemann, M. Brinkmann, T. Pfohl, and S. Herminghaus, Droplet based microfluidics, Rep. Prog. Phys. **75**, 016601 (2011).

[28] S. L. Anna, Droplets and bubbles in microfluidic devices, Annu. Rev. Fluid Mech. **48**, 285 (2016).

[29] L. Shang, Y. Cheng, and Y. Zhao, Emerging droplet microfluidics, Chem .Rev. **117**, 7964 (2017).

[30] K. Doufène, C. Tourné-Péteilh, P. Etienne, and A. Aubert-Pouëssel, Microfluidic systems for droplet generation in aqueous continuous phases: A focus review, Langmuir **35**, 12597 (2019).

[31] T. Cubaud and T. G. Mason, Capillary threads and viscous droplets in square microchannels, Phys. Fluids **20**, 053302 (2008).

[32] S. Jakiela, S. Makulska, P. M. Korczyk, and P. Garstecki, Speed of flow of individual droplets in microfluidic channels as a function of the capillary number, volume of droplets and contrast of viscosities, Lab Chip **11**, 3603 (2011).

[33] M. Moiré, Y. Peysson, B. Herzhaft, N. Pannacci, F. Gallaire, L. Augello, C. Dalmazzone, and A. Colin, Ultralow interfacial tension measurement through jetting/dripping transition, Langmuir **33**, 2531 (2017).

[34] T. Helmers, P. Kemper, J. Thöming, and U. Mießner, The flow topology transition of liquid–liquid Taylor flows in square microchannels, Exp. Fluids **63**, 5 (2022).

[35] T. Dinh and T. Cubaud, Role of interfacial tension on viscous multiphase flows in coaxial microfluidic channels, Langmuir **37**, 724 (2021).

[36] M. Hashimoto, P. Garstecki, H. A. Stone, and G. M. Whitesides, Interfacial instabilities in a microfluidic Hele-Shaw cell, Soft Matter **4**, 1403 (2008).

[37] S. A. Khan and S. Duraiswamy, Microfluidic emulsions with dynamic compound drops, Lab Chip **9**, 1840 (2009).

[38] X. Chen and C. L. Ren, Experimental study on droplet generation in flow focusing devices considering a stratified flow with viscosity contrast, Chem. Eng. Sci. **163**, 1 (2017).

[39] N. M. Kovalchuk and M. J. H. Simmons, Review of the role of surfactant dynamics in drop microfluidics, Adv. Colloid Interface Sci. **312**, 102844 (2023).

[40] T. Cubaud, B. Conry, X. Hu, and T. Dinh, Diffusive and capillary instabilities of viscous fluid threads in microchannels, Phys. Rev. Fluids **6**, 094202 (2021).

[41] T. Cubaud, Swelling of diffusive fluid threads in microchannels Phys. Rev. Lett. **125**, 174502 (2020).

[42] M. J. Madou, Fundamentals of Macrofabrication and Nanotechnology, Vol II (CRC Press, Boca Raton, FL, 2012).

[43] X. Hu and T. Cubaud, Inertial destabilization of highly viscous microfluidic stratifications, Phys. Rev. Fluids **1**, 044101 (2016).

[44] T. Cubaud, B. M. Jose, S. Darvishi, and R. Sun, Droplet breakup and viscosity-stratified flows in microchannels, Int. J. Multiphase Flow **39**, 29 (2012).

[45] T. Cubaud, Segmented flows of viscous threads in microchannels, Phys. Rev. Fluids **4**, 084201 (2019).